Check for updates

Geophysical Research Letters

RESEARCH LETTER
10.1029/2021GL097114

Key Points:

- Sudden increase in Greenland freshwater release is turned into century scale change by deep ocean dynamics
- Upper ocean responses to moderately enhanced freshwater release from Greenland reverse on the same timescale once release ceases
- Ocean model formulation affects regional expressions but basin-scale responses are robust, so is the timing on decadal to centennial scales

Supporting Information:

Supporting Information may be found in the online version of this article.

Correspondence to:

T. Martin,
tomartin@geomar.de

Citation:

Martin, T., Biastoch, A., Lohmann, G., Mikolajewicz, U., & Wang, X. (2022). On timescales and reversibility of the ocean's response to enhanced Greenland Ice Sheet melting in comprehensive climate models. *Geophysical Research Letters*, *49*, e2021GL097114. https://doi.org/10.1029/2021GL097114

Received 3 DEC 2021
Accepted 4 FEB 2022

© 2022. The Authors.
This is an open access article under the terms of the Creative Commons Attribution-NonCommercial-NoDerivs License, which permits use and distribution in any medium, provided the original work is properly cited, the use is non-commercial and no modifications or adaptations are made.

On Timescales and Reversibility of the Ocean's Response to Enhanced Greenland Ice Sheet Melting in Comprehensive Climate Models

Torge Martin[1], Arne Biastoch[1,2], Gerrit Lohmann[3], Uwe Mikolajewicz[4], and Xuezhu Wang[3,5]

[1]GEOMAR Helmholtz-Zentrum Für Ozeanforschung Kiel, Kiel, Germany, [2]Christian-Albrechts-Universität Kiel, Kiel, Germany, [3]Alfred-Wegener-Institut Helmholtz-Zentrum Für Polar- und Meeresforschung, Bremerhaven, Germany, [4]Max-Planck-Instiut Für Meteorologie, Hamburg, Germany, [5]Now at College of Oceanography, Hohai University, Nanjing, China

Abstract Warming of the North Atlantic region in climate history often was associated with massive melting of the Greenland Ice Sheet. To identify the meltwater's impacts and isolate these from internal variability and other global warming factors, we run single-forcing simulations including small ensembles using three complex climate models differing only in their ocean components. In 200-year-long preindustrial climate simulations, we identify robust consequences of abruptly increasing Greenland runoff by 0.05 Sv: sea level rise of 44 ± 10 cm, subpolar North Atlantic surface cooling of 0.7°C, and a moderate AMOC decline of 1.1–2.0 Sv. The latter two emerge in under three decades—and reverse on the same timescale after the perturbation ends in year 100. The ocean translates the step-change perturbation into a multidecadal-to-centennial signature in the deep overturning circulation. In all simulations, internal variability creates notable uncertainty in estimating trends, time of emergence, and duration of the response.

Plain Language Summary Enhanced melting of Greenland's glaciers is considered to be a major player in past rapid climate transitions and anticipated to soon impact ocean circulation under current global warming. Global warming triggers complex processes and feedbacks, of which greater amounts of meltwater slowing the large-scale ocean circulation is only one. To better understand the sensitivity of the real but also the model ocean to just this meltwater, we run idealized experiments with up-to-date climate models, which use the same atmosphere and land but different ocean components. We find that sea level rise, cooling of the North Atlantic region, and slowing of the ocean circulation are responses common to all models while regional magnitudes of these responses differ considerably. Once we stop adding freshwater, all three models show that surface temperature and ocean circulation recover as quickly (or slowly) as they changed at the beginning of the experiment. Sea level rise is a lasting impact though.

1. Introduction

Increasing mass loss of the Greenland Ice Sheet (GrIS) under global warming (Mouginot et al., 2019; The IMBIE Team, 2020) has sparked a growing interest in and concern about the impact of the associated freshwater (FW) release on the ocean circulation. This is because the ice sheet's deterioration and consequences thereof are considered a tipping element in Earth's climate (Lenton et al., 2008 & 2019). Being a key element in rapid climate transitions, massive FW release into the subpolar North Atlantic (SPNA) has weakened or shut off the Atlantic Meridional Overturning Circulation (AMOC) with global implications in the past (Hawkins et al., 2011; Hu et al., 2011; Rahmstorf, 2002). The FW has the potential to increase stratification in the SPNA such that processes of density gain, for example, heat loss to the atmosphere and sea-ice formation, become less effective in forming deep water, which is a key element of the AMOC.

Ice-core records from GrIS show rapid warming events of about 10°C on a decadal timescale during the last glacial as part of the so-called Dansgaard-Oeschger cycle on a millennial timescale (Bond et al., 1993; Dansgaard et al., 1993; NGRIP, 2004; Severinghaus & Brook, 1999). These sudden temperature reversals are accompanied by opposing cooling in the southern hemisphere, which is recorded in Antarctic ice cores with a time lag of about 200 years (WAIS Divide Project Members, 2015). The Dansgaard-Oeschger cycle as well as the rapid Greenland warming itself have been tied to large-scale ocean processes, AMOC variations (e.g., Broecker et al., 1990), and open ocean deep convection in the Nordic Seas (Dokken et al., 2013). The bipolar seesaw of contrasting

temperature evolution in the northern and southern hemispheres can be driven by deep-water formation variations (Broecker, 1998) or linked to an interior ocean heat reservoir (Pedro et al., 2018; Stocker & Johnsen, 2003) though this is still under debate (Dima et al., 2018). While causes and mechanisms creating the centennial lag between Greenland and Antarctica need to be further elucidated, the bipolar seesaw suggests a prominent role of the ocean circulation.

With the onset of the 21st century, the annual mass balance of GrIS turned continuously negative and experienced record losses in 2011, 2012, and 2019 (Hanna et al., 2021; The IMBIE Team, 2020). The FW flux from GrIS is estimated at about 750 km^3/yr (0.024 Sv) over the second half of the 20th century and has increased roughly by 300 km^3/yr (0.01 Sv) over the last two decades (Bamber et al., 2018). This magnitude still is three times less than Arctic river discharge or liquid FW export through either Davis or Fram Strait (Haine et al., 2015); neither high-resolution ocean hindcasts (Böning et al., 2016) nor observations (Rhein et al., 2018) have demonstrated a significant impact on SPNA deep water formation, yet. However, a further increase by 0.005–0.01 Sv can be expected over the next couple of decades (Golledge et al., 2019; Haine et al., 2015). Is this sufficient to trigger a lasting ocean response? And is the response reversible as soon as the melting stabilizes or reduces?

Inspired by ocean-only model intercomparisons showing a significant spread in AMOC mean state but nevertheless similar responses to variability in the atmospheric forcing (Danabasoglu et al., 2014 & 2016), we here investigate the role of ocean model implementations in simulating the response to rapid GrIS melting in coupled climate models. Designated multimodel comparisons are rare and show significant model spread (e.g., Swingedouw et al., 2013 & 2015). Often, it is unclear whether uncertainty arises from atmosphere or ocean model biases. Arguing that ocean processes and feedbacks dominate the long-term implications, we here expose three climate models using the same atmosphere/land components but different ocean/sea-ice model physics as well as grids to the same FW-release.

With this study, we address three leading objectives related to both past and future rapid climate change involving a FW perturbation of the AMOC: (1) proving that the meridional overturning circulation is translating a sudden, step-like change in ocean boundary conditions into a centennial-scale global climate response, (2) characterizing implications of enhanced FW release from GrIS as a tipping element, that is, a nonreversible process, in the climate system, and (3) identifying robust climate responses in single-forcing ensemble simulations considering diverging ocean model formulations.

2. Models and Experiments

In this study, we compare simulations of three climate models: MPI-ESM, FOCI, and AWI-CM. The models use the same atmosphere and land components, ECHAM6.3 (Stevens et al., 2013) and JSBACH (Reick et al., 2013), on the same 6T3-grid (∼1.9°) but differ in their ocean and sea-ice models. The MPI-ESM (Mauritsen et al., 2019) is used in the well-established set up MPI-ESM1.2-LR, a contribution to CMIP6, including the MPI-OM ocean and sea-ice model with a nominal ocean grid resolution of 1.5° (GR15); the grid with the North Pole centered on Greenland yields an actual grid spacing of 15–60 km in the Nordic Seas and SPNA (Jungclaus et al., 2013). FOCI version 1 (Matthes et al., 2020) is based on the MPI-ESM infrastructure but applying the NEMO3.6 and LIM2 ocean and sea-ice models instead. For the ocean, the ORCA05 grid is used having a grid spacing of 0.5° with the North Pole stretched across the Arctic yielding an effective grid spacing of 25–40 km in the Nordic Seas and SPNA. The AWI-CM used here (Lohmann et al., 2020; Sein et al., 2018; Sidorenko et al., 2015) is based on the FESOM ocean and sea-ice model, which is applied to an irregular mesh of globally 1° and higher resolution of about 45 km near the equator and 25 km north of 45°N (termed LR or FESOM-CORE-2 mesh). Since all models are optimized to their own preindustrial climate equilibrium, climate parameter choices, also in the atmosphere, may slightly diverge. Nevertheless, all models make use of the same physics in the atmosphere and land components and also are of comparable, full complexity in the ocean and sea ice. All models are applied to horizontal ocean grids demanding parameterization of mesoscale eddies and vertical z-grids with linear free-surface.

To investigate the ocean climate response to enhanced GrIS-melting, we conduct a suite of idealized FW perturbation experiments. In contrast to former so-called hosing experiments, we refrain from a broad basin-scale FW release but instead prescribe a spatially most realistically distributed FW flux directly along the coast of Greenland (see Figure S1 in Supporting Information S1). Since our objective is to demonstrate the influence of ocean model formulation, we are aiming to trigger a significant but moderate response. Thus, we chose to prescribe a

more realistic and weaker than usual FW perturbation of 0.05 Sv on annual mean, which is achieved by appropriate scaling of the present-day mean Greenland FW flux (Bamber et al., 2012) preserving spatial and seasonal heterogeneity (see Methods in Supplementary).

All model experiments are conducted under preindustrial climate conditions and start from an equilibrium model state after a spin-up of 1500 years or more. A 300-year long PI-control run (AWI-CM only 200 years) is conducted for reference. Perturbation experiments extend over 200 years with 0.05 Sv of FW added from year 1 to year 100. Expecting a rather weak response of the AMOC to the FW perturbation, we run a small 3-member ensemble with both, MPI-ESM and FOCI, to separate the response from internal climate variability. A single realization of the AWI-CM is included as it was just an experiment of opportunity. An additional experiment with a doubled FW perturbation of 0.1 Sv using FOCI is included to demonstrate the sensitivity of the modeled AMOC.

3. Results

We focus on robust changes to sea level, the AMOC, and surface as well as deep ocean temperature as consequences to the FW perturbation and cornerstones of any global climate change. Magnitudes, timescales, and reversibility of the responses are discussed. Pathways of FW redistribution are found in manometric sea level change and confirmed by a passive tracer analysis. Responses to the FW perturbation are presented as 50-year means typically taken over model years 50–99 or 75–125 depending on whether the quantity reaches a quasi equilibrium during the perturbation period or rather exhibits a peak change at the end.

3.1. Sea Level Change

Global mean sea level change (SLC) in our experiments can be estimated up front by a back-of-the-envelope calculation: Applying a continuous annual-mean FW flux of 0.05 Sv over 100 years to an ocean with an approx. surface area of 361×10^6 km^2 will yield a linear global-mean barystatic sea level rise of about 0.44 m. Consistently, modeled global-mean sea level, which is the total of barystatic sea level and global-mean thermosteric sea level, rises linearly during the first 100 years of the experiment, the perturbation period, and then equilibrates at 0.44 ± 0.005 m (Figure 1a). The thermosteric contribution is found to be statistically significant but of rather negligible magnitude (0.006 ± 0.001 m). Barystatic sea level rise is clearly nonreversible on the timescales considered here. Computation of SLC components follow the definitions of Gregory et al. (2019); details are provided in the Supporting Information S1.

The FW input triggers sea level responses at three different timescales. First, there is the already mentioned immediate increase in the global ocean volume by barystatic SLC. Second, releasing the FW from Greenland yields a multidecadal response in regional dynamic sea level (DSL) affecting most of the North Atlantic (Figure 2a) with major contributions by steric changes (see also Figure S2 in Supporting Information S1). Third, steric and manometric adjustments outside the North Atlantic last far beyond the centennial timescale of our experiments (Figure S2 in Supporting Information S1) and are mostly associated with the export of the FW with the deep western boundary current and further with the Antarctic Circumpolar Current (Figure S3, S4 in Supporting Information S1).

In all perturbation experiments, a significant and robust increase in basin-mean DSL of 0.03–0.05 m between 40°N and 65°N emerges within the first three decades (Figure S2 in Supporting Information S1). The timing varies, which could be related to individual model characteristics but variations within the MPI-ESM and FOCI ensembles also point at internal (multi-)decadal variability masking the signal. Internal variability is most pronounced in the MPI-ESM simulations. Diverging expressions of variability associated with the North Atlantic Current and the subpolar gyre (SPG) among the models play an important role in this and are also visible in the spatial pattern of DSL change (Figure 2a). In the MPI-ESM experiments, we find a major reduction of the barotropic stream function in the south-eastern half of the SPG (yellow contour in Figure 2a; cf. Figure S5 in Supporting Information S1) relating to the dominant DSL decline, indicating an intensifying and expanding SPG, and a more zonal path of the North Atlantic Current under FW perturbation. In FOCI, a similar though less prominent expansion of the SPG occurs but on the north-eastern side of the gyre. Instead, FOCI and AWI-CM yield a slight weakening of the western SPG (Figure S5 in Supporting Information S1). Moreover, AWI-CM shows a weakening but northward expansion of the subtropical gyre yielding reduced DSL at 25–35°N and increased around 40–45°N (Figure 2a).

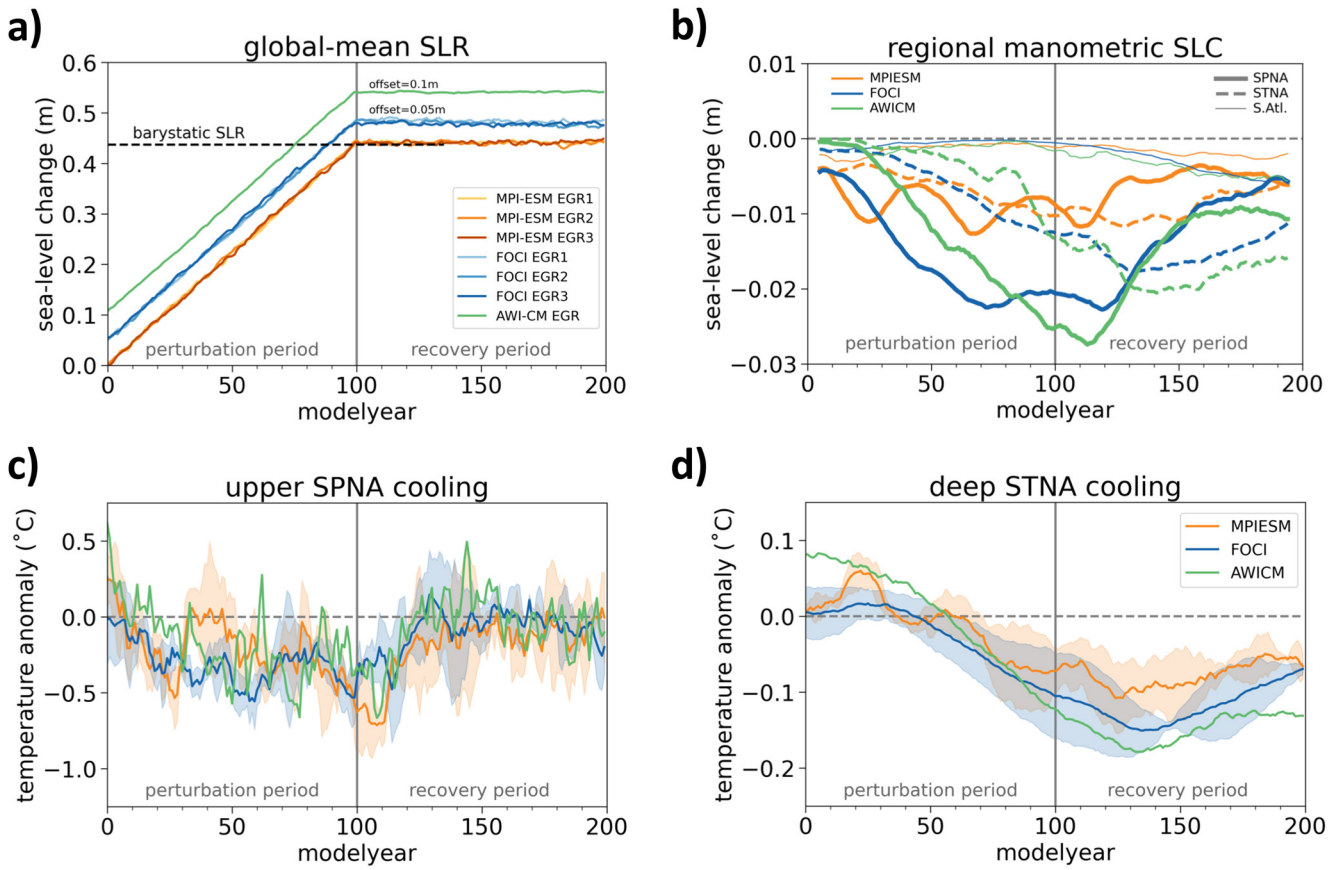

Figure 1. (a) Time series of global-mean sea level rise (SLR) as a consequence of the freshwater perturbation of 0.05 Sv over 100 years. The black dashed line indicates the barystatic contribution. Lines for FOCI and AWI-CM are shifted upward for visibility. (b) Low-pass filtered (11-year running mean) time series of manometric sea level change (SLC) for the subpolar North Atlantic (40°-65°N, bold solid lines), the subtropical North Atlantic (15°-40°N, dashed), and the equatorial plus southern Atlantic (30°S-15°N, thin solid). Here, the ensemble mean is shown for MPI-ESM and FOCI. (c) Time series of upper subpolar North Atlantic potential temperature (averaged over 0–1,000 m); see the solid box in Figure 4b. (d) Time series of deep subtropical North Atlantic (1,500–3,500 m, 15°-40°) potential temperature; see the dashed box in Figure 4b. In both panels (c) and (d), shading indicates ensemble spread in MPI-ESM and FOCI experiments showing ±1σ deviation of members from ensemble mean (bold line).

Nevertheless, a common response simulated by all models is an increase in DSL of 4–7 cm along the North American east coast extending from the Baffin Bay to the Mid-Atlantic Bight and in the eastern North Atlantic (Figure 2a) though here the increase differs strongly by an order of magnitude. The spatial extent of SLC also differs, stays off the European shelf in AWI-CM but reaches the coast in FOCI. DSL change already illustrates that some of the FW escapes from the SPG into the subtropical gyre in MPI-ESM and FOCI but less prominently in AWI-CM. The FW follows the "FW leakage" along the Canary current on the eastern side of the Atlantic discussed by Swingedouw et al. (2013). Matching the intensity of this leakage, the impact on the subtropical North Atlantic is model dependent being expressed most strongly in the MPI-ESM and least in the AWI-CM (Figure S2 in Supporting Information S1, dashed lines). Lastly, DSL change in the SPNA reverses after the perturbation is stopped in all cases on roughly the same decadal timescale as it emerged after the start of the experiment (Figure S2 in Supporting Information S1, bold lines) though internal variability hinders the exact computation of the timing.

The lasting, centennial-scale response is best seen in manometric SLC. All three models simulate a gradual decline in local mass for the deep subpolar North Atlantic (40°–65°N) over the extent of the perturbation period—except that the signal is partly masked by internal variability in the MPI-ESM runs as discussed above (Figure 1b, bold lines). The decrease in ocean mass illustrates an accumulation of the FW in the SPG replacing more saline waters. This is a regional change relative to the reference run excluding the global mean barystatic SLC, which otherwise would clearly dominate the manometric component. While DSL change is positive, that is, the SPG becomes less

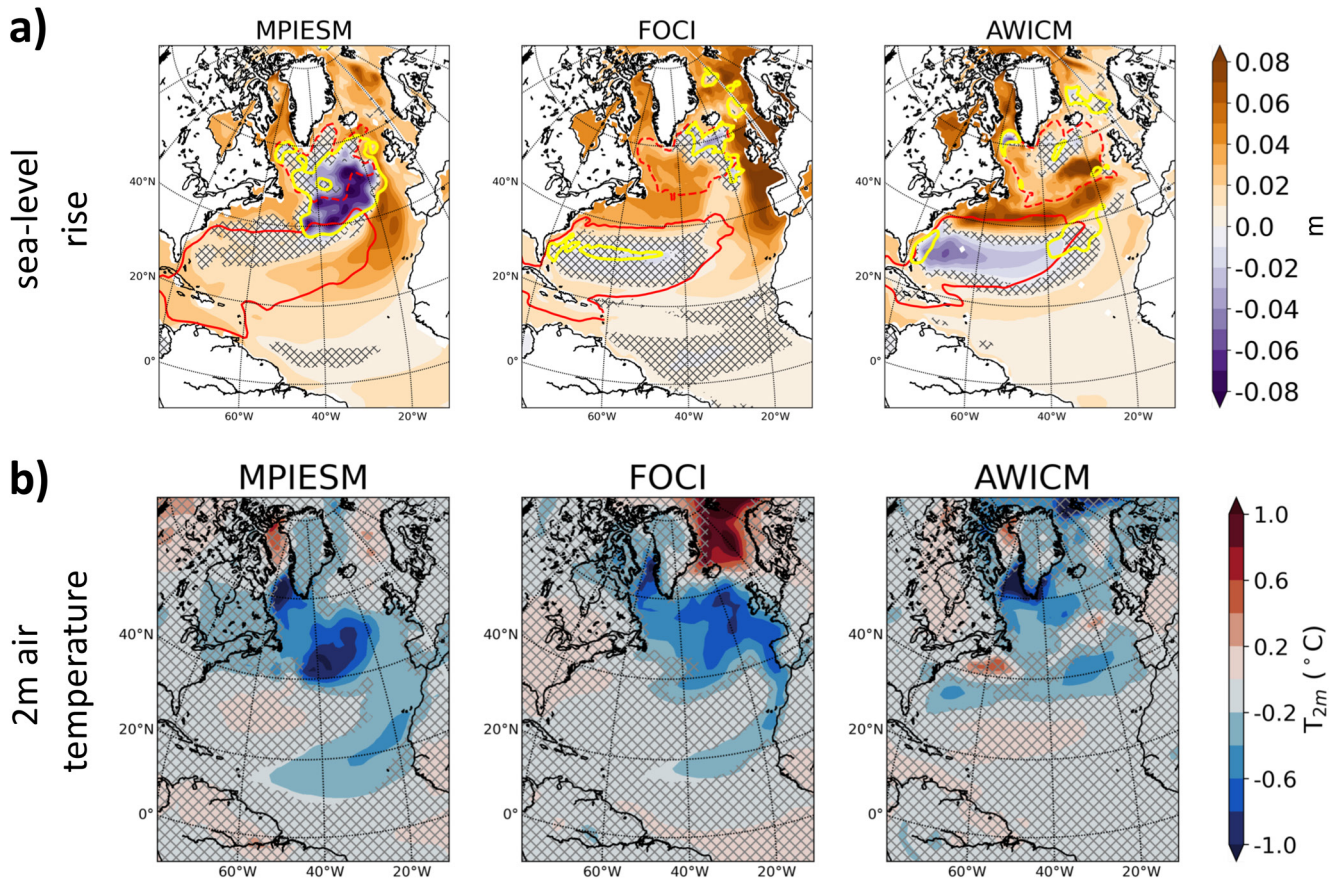

Figure 2. (a) Ocean dynamic sea level change averaged over years 75–125. Red lines depict +10 (solid) and −10 Sv (dashed) contours of the reference mean state barotropic stream function marking the subtropical and subpolar gyres, respectively (cf. Figure S5 in Supporting Information S1). Yellow lines are contours of −1 Sv change in barotropic stream function. (b) Change in air temperature at 2 m averaged over years 50–99. Changes are computed as deviations from the overall mean of reference run using ensemble means for MPI-ESM and FOCI. Hatching masks non-significant change ($p = 0.95$).

divergent as the density gradient across its boundary diminishes, regional steric SLC exceeds DSL change stating a decrease in water column mass as FW enters the SPNA. Mass is continuously leaked to the subtropical North Atlantic and Arctic Oceans. We thus see manometric SLC in the subtropics (15°–40°N) also declining reaching a minimum 3–4 decades after the SPNA (dashed lines). The simulations are just long enough to show that also this response in the subtropics is reversing on the same timescale. A passive tracer tagging the FW released from Greenland shows that a fraction of the FW is parting south at the eastern side of the Atlantic, joining the subtropical gyre with the Canary and North Equatorial Currents, and recirculating in the gyre at intermediate depth (Figure S4 in Supporting Information S1). At the same time, the FW is entrained into North Atlantic Deep Water, accumulating in the deep subpolar basin, and being exported south from the North Atlantic with the deep western boundary current (Figure S4c in Supporting Information S1). This causes a gradual decrease in manometric SLC in the equatorial and southern Atlantic, which keeps evolving beyond the 200-year-long experiments (Figure 1b, thin lines) and eventually also reaches the other ocean basins (see Figure S3 in Supporting Information S1).

3.2. AMOC Weakening

In response to the FW-induced density decrease in the upper SPNA, stratification increases and less deep water is formed, which shows as reduced deep mixing in both, Labrador and Nordic Seas (Figure S6 in Supporting Information S1). Enhanced deep mixing in the Irminger Sea (in FOCI and AWI-CM) cannot compensate (cf. Devilliers et al., 2021). In consequence, the AMOC weakens rapidly within a couple of decades with a new mean state emerging in years 11–21 (Figure 3). As we apply a moderate FW forcing of 0.05 Sv, all three models yield a relatively weak reduction in AMOC strength (defined as the vertical maximum of the stream function at

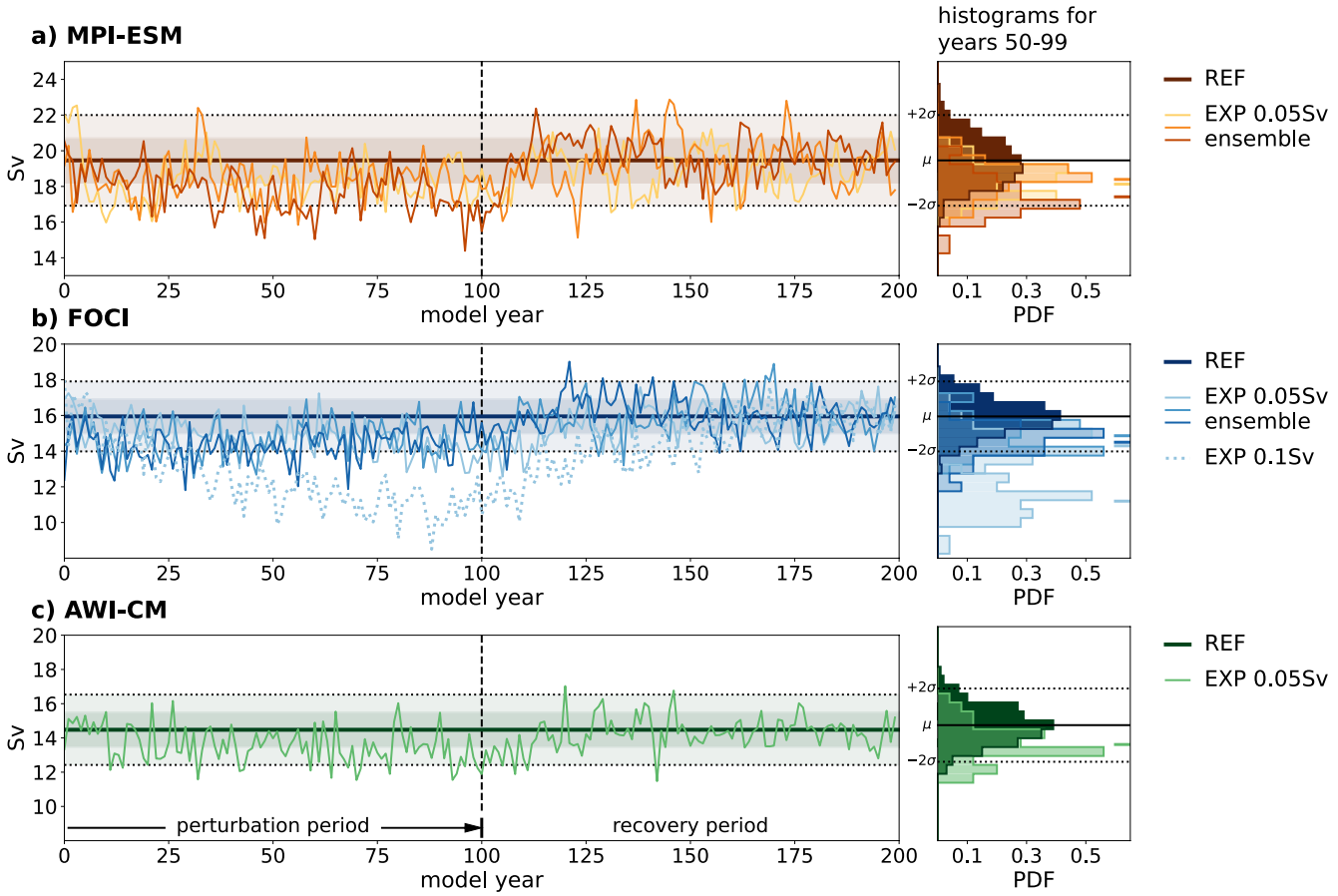

Figure 3. Response in Atlantic Meridional Overturning Circulation (AMOC) strength to the freshwater perturbation in (a) MPI-ESM, (b) FOCI, and (c) AWI-CM. Time series shows annual mean AMOC strength of the perturbation experiments. Long-term mean reference AMOC strength is shown as a bold straight line in the background of each panel along with shading for standard deviation (darker ±1σ, lighter ±2σ) of PI-control interannual variability. Histograms on the right depict the respective distributions of the annual mean AMOC strength from the reference run using the entire time series and for the perturbation experiments using the last 50 years of the perturbation period (years 50–99); bin width is 0.5 Sv and consistent color coding is applied; a short horizontal line on the very right in the histogram plots marks the respective mean of each distribution. AMOC strength is defined as the vertical maximum of the zonal mean meridional stream function in the North Atlantic, here at 26.5°N. Panel (b) also includes the results of the 0.1 Sv freshwater perturbation experiment with FOCI as dashed time series and bright blue histogram.

a given latitude). Sampling the model output at the latitude of the RAPID observational array (26.5°N) and averaging over the years 50–99, the weakening varies among ensemble members: 1.1–2.0 Sv (MPI-ESM), 1.1–1.5 Sv (FOCI), and 1.1 Sv AWI-CM (Figure 3). The decline is a little larger, 1.3–2.4 Sv, at the models' individual overall AMOC maximum near 35°N (Figure 4a). Interestingly, the model with the strongest AMOC and largest interannual variability in the reference run (MPI-ESM: 19.5 ± 1.3 Sv) is most sensitive to the FW perturbation (cf. FOCI: 16.0 ± 1.0 Sv, AWI-CM: 14.5 ± 1.0 Sv; see bold constant line and shading in Figure 3). Although relatively weak considering standard deviations of 1.0–1.3 Sv of the annual mean time series, the AMOC response measured as mean over the last 50 years of the perturbation period (years 50–99) is significant in all cases.

The Atlantic cross section of the AMOC stream function in Figure 4a reveals that the entire overturning cell is affected. The decrease in transport magnitude is most extensive in the MPI-ESM ensemble mean, even hinting at an expanding bottom cell (blue shading extending across zero contour of reference mean state). In contrast, the decline does not affect the deepest part of the deep AMOC return flow in the AWI-CM, which also has the most extensive AMOC cell.

Perturbing FOCI with twice the amount of FW (0.1 Sv), a more typical magnitude for hosing experiments, we find a stronger AMOC weakening of −4.8 Sv at 26.5°N and averaging over years 50–99 (Figure 3, dotted blue line and light blue histogram). The trend in AMOC decline over the first two decades resembles that of the weaker

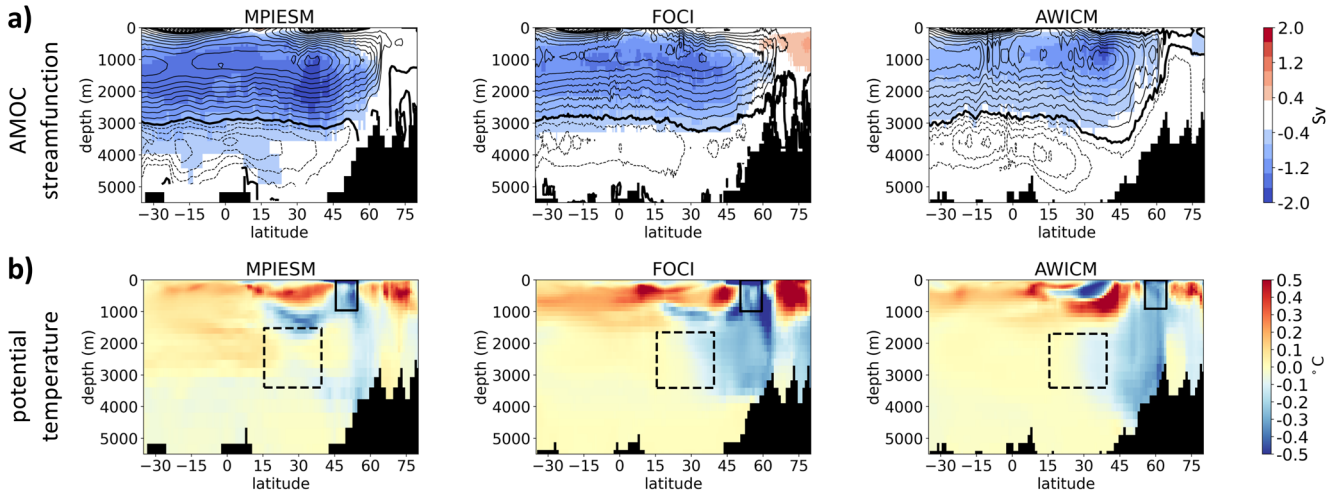

Figure 4. (a) The long-term mean reference state of the meridional overturning circulation in the Atlantic (black contours) and its response to the freshwater perturbation (colors). (b) Change in zonal mean potential temperature for the Atlantic Ocean due to freshwater perturbation. Differences are computed based on an average of years 50–99 of the experiments using ensemble means for MPI-ESM and FOCI.

forcing, that is, the time of emergence is similar, but the decline continues and the new quasi-equilibrium state is reached only after 3–4 decades.

Further, our experiments show that the AMOC weakening is reversible on the same decadal timescale as the decline occurred once the additional FW flux ceases. This also holds for the twice as strong perturbation. A small overshoot can be observed before the reference equilibrium strength of the PI-control state is reached again.

3.3. Ocean Cooling

The weaker AMOC transports less heat and salt northward, effectively cooling the SPNA (Drijfhout et al., 2012) and reinforcing the freshening. Despite the relatively weak response of the AMOC, the experiments yield a significant upper ocean (0–1,000 m) and surface cooling of 0.3°C and 0.7°C in ocean potential temperature (Figures 1c and 4b) and 2m air temperature (Figure S7 in Supporting Information S1), respectively, in the SPNA region averaged over years 50–99. Being tightly linked to the AMOC decline, the ocean cooling occurs rapidly within 1–2 decades into the perturbation period, air temperature declines faster. As the AMOC recovers, so does SPNA temperature. Surface warming takes a decade longer than the initial cooling (Figure S7 in Supporting Information S1). The FW perturbation quickly increases stratification yielding a rapid decoupling of the atmosphere and surface ocean from warmer layers underneath. As the system recovers after the perturbation is stopped, the upper ocean needs to warm, which is slower. All three models agree very well on magnitude and timescale of the cooling and its reversal despite the differences in ocean model formulations, the spatial patterns differ, however.

Maps in Figure 2b show the divergence of the quasi-equilibrium state during the perturbation period (averaged years 50–99) from the mean state of the reference runs. The surface cooling exceeds 1°C in some locations. Weak in magnitude (<0.4°C) but significant cooling also occurs over the FW leakage into the subtropical gyre in the MPI-ESM and FOCI simulations. Warming over the Nordic Seas is not a robust feature but model specific to FOCI—Figure 2b shows 2 m air temperature smoothing the underlying SST signal. FOCI simulates the strongest reduction in deep convection (Figure S6 in Supporting Information S1), the response is also found in MPI-ESM but weaker and not significant, and AWI-CM maintains intense deep convection only reduced in extent. Further, the cooling over the North Atlantic Ocean does not expand to adjacent continents in our simulations—changes in air temperature over land are not significant. Given the weak AMOC response, there is no related significant surface warming at lower latitudes or in the South Atlantic. Such heat backlog is a potential but debated consequence of a (much stronger) slackening of the AMOC (Crowley, 1992; Pedro et al., 2018; Seidov & Maslin, 2001). This agrees with earlier studies, in which complex models showed similarly weak or nonrobust SST and 2 m air-temperature responses even at larger FW forcing (Kageyama et al., 2013; Swingedouw et al., 2013).

The surface cooling in the SPNA is imposed on the characteristics of the North Atlantic Deep Water and exported southward with the AMOC. This can be well seen in a cross section of Atlantic zonal mean potential temperature in Figure 4b. The sections also reveal considerable differences in the response and dynamics of the subtropical North Atlantic between 100 and 1,000 m, which are beyond the scope of this study. When the North Atlantic Deep Water (at depths of 1,500–3,000m) reaches subtropical latitudes (15°–40°N, dashed box in Figure 4b), the timescale of the response to the sudden FW perturbation has changed to centennial. The cooling starts in the 4th decade and temperatures decline below the reference level not before year 50 (Figure 1d) reaching a minimum temperature deviation of 0.9–1.8°C decades after the perturbation has stopped. Both, FOCI and AWI-CM, feature deep convection in the SPNA exceeding 1,500 m (Figure S6 in Supporting Information S1). This carries the cooling (and freshening) signal to the deep SPNA, then spreading southward along the western boundary (Figure S8 in Supporting Information S1). In contrast, the MPI-ESM has shallower deep mixing and exhibits a slight increase in the bottom cell (Figure 4a). Here, an expanding AABW volume contributes to the deep cooling at the interface of the overturning cells (Figures 4b and S8a in Supporting Information S1). Nevertheless, the passive tracer tagging the FW perturbation has similar patterns at 2000 m in both, MPI-ESM and FOCI (Figure S4 in Supporting Information S1).

The reversal, that is, warming, begins 30–40 years into the recovery period having similar (FOCI) or smaller warming trend magnitudes (MPI-ESM and AWI-CM) than the cooling. Contrasting the upper SPNA response, this graph highlights the role of the deep ocean in translating a rapid climate change centered on Greenland into a centennial signal eventually reaching the Southern Ocean after a couple of centuries.

4. Conclusions

We exposed three global climate models with different oceans but same atmosphere components and overall similar, noneddying grid resolution to the same FW perturbation mimicking enhanced Greenland meltwater runoff equivalent to almost 0.5 m of sea level rise over a century. Regarding the three leading objectives defined in the introduction, we demonstrated that.

1. Robust large-scale response exists in both magnitude and timescales of major impacts, such as AMOC weakening, subpolar North Atlantic surface cooling, and deep ocean perturbation export—significant regional differences in the pattern and thus local magnitude of the response are found nonetheless; while this is reassuring for paleo applications of such models focusing on dominant responses on timescales beyond several decades, this is discomforting regarding future decadal predictions of, for instance, coastal sea level rise.
2. Even significantly enhanced FW input from GrIS at a magnitude to be roughly expected by the end of the 21st century is not necessarily a tipping point in climate change—AMOC weakening and associated surface cooling reverse to control state within a couple of decades after ceasing of the perturbation, which is about the timescale of their initial response to the FW release.
3. The ocean effectively translates a rapid melt or disintegration event of GrIS on interannual timescale into a centennial response in temperature and salinity in the deep North Atlantic—this change is eventually exported on the same timescale to the southern hemisphere and other ocean basins; depending in the magnitude and duration of the FW release, this may ultimately also affect Antarctic climate and relate to the centennial lag between Greenland and Antarctic ice-core records during Marine Isotope Stage 3 (WAIS Divide Project Members, 2015; Pedro et al., 2018).

These conclusions are based on the models presented. AMOC sensitivity to freshwater and global warming varies significantly among climate models (Bellomo et al., 2021; Stouffer et al., 2006). Considerable differences in internal variability and regional response patterns complicate the quantification of the added FW's impact. This is in itself a notable result as it underlines the importance of providing uncertainty estimates with climate projections on, for instance, regional sea level and temperature change. Some robust estimates for key quantities can be provided nevertheless:

1. Sterodynamic SLC in the North Atlantic can add 10 cm to the global mean expansion of 44 cm; this addition is particularly large on the continental shelves emphasizing the vulnerability of coastal regions to dynamic and manometric effects in SLC due to added FW.

2. The AMOC weakens rapidly with 1–2 decades in response to the sudden FW perturbation; the reduction of 1.1–2.0 Sv at 26.5°N is relatively small (≤10%); global warming effects aside from GrIS melting are projected to cause an AMOC weakening of 6–8 Sv (34%–45%) by 2100 (Weijer et al., 2020) and a warmer SPNA may be less susceptible to GrIS meltwater (Swingedouw et al., 2015).
3. As a consequence, the SPNA region cools by 0.7°C and 0.3°C at the sea surface and averaged over the upper 1000 m; local temperature change can be as large as 1.2°C on a 50-year mean.

Internal variability, in particular, at the surface and in the upper ocean is found to be of similar magnitude as the perturbation response. In particular, the time of emergence is often difficult to estimate due to the noise. Running large ensembles is a viable solution. This highlights the foreseeable difficulties in detecting and attributing current changes in the North Atlantic to the ongoing acceleration of melting of the Greenland Ice Sheet as has been indicated by other studies as well (e.g., Böning et al., 2016; Devilliers et al., 2021). Despite these difficulties, we anticipate that the ocean will respond already to moderate increases in ice-sheet mass loss, will stabilize in its new state as the freshwater input stabilizes, and will—to a large degree—reverse to its old state on predictable timescales once enhanced ice sheet stabilizes.

Data Availability Statement

Model code: The **MPI-ESM1.2** is available at https://www.mpimet.mpg.de/en/science/models/mpi-esm/ under the Software License Agreement version 2 after acceptance of a license (https://mpimet.mpg.de/en/science/modeling-with-icon/code-availability). **FOCI1** is composed of several components, which prohibit to distribute the full source code due to licensing issues; ECHAM6.3 is provided by the MPI-M (https://mpimet.mpg.de/en/science/models/mpi-esm/echam); NEMO3.6 (rev. 6721) is available at https://forge.ipsl.jussieu.fr/nemo/svn/NEMO/releases/release-3.6/NEMOGCM; FOCI-specific code changes and runtime environment are provided at http://doi.org/10.5281/zenodo.3568061 (see Matthes et al., 2020). The **AWI-CM** as documented at https://fesom.de/models/awi-cm/uses ECHAM6.3 (see above) and FESOM1.4 (https://fesom.de/models/fesom14/). *Data and software*: Model output from all experiments and the Jupyter notebooks required to re-produce the analysis and figures are available through GEOMAR at https://hdl.handle.net/20.500.12085/b4c3bc18-1a1d-49f2-8310-a0cef2b00b9b.

Acknowledgments
TM, AB, UM, and GL conceived together the idea for the experimental setup and all contributed to writing the manuscript. TM analyzed the model output and created the figures. UM, TM, and XW performed the model experiments with MPI-ESM, FOCI, and AWI-CM, respectively. We thank two anonymous reviewers for their helpful comments in improving the final manuscript. TM thanks Jan Harlaß for his help in implementing the meltwater runoff forcing in FOCI and Sebastian Wahl for helping to set up FOCI. This study was funded by the German Federal Ministry of Education and Research (BMBF) as a Research for Sustainability initiative (FONA) through the project PalMod: From the Last Interglacial to the Anthropocene – Modeling a Complete Glacial Cycle; WP1.2.2: Scale Interactions: Analysis of ocean dynamics (FKZ: 01LP1503D). The work was supported by the North-German Supercomputing Alliance (HLRN) and Deutsches Klimarechenzentrum (DKRZ) providing computational resources and technical support. Open access funding enabled and organized by Projekt DEAL.

References

Bamber, J. L., van den Broeke, M., Ettema, J., Lenaerts, J., & Rignot, E. (2012). Recent large increases in freshwater fluxes from Greenland into the North Atlantic. *Geophysical Research Letters*, *39*, L19501. https://doi.org/10.1029/2012GL052552

Bamber, J. L., Tedstone, A. J., King, M. D., Howat, I. M., Enderlin, E. M., van den Broeke, M. R., & Noel, B. (2018). Land ice freshwater budget of the Arctic and North Atlantic oceans: 1. Data, methods, and results. *Journal of Geophysical Research: Oceans*, *123*, 1827–1837. https://doi.org/10.1002/2017jc013605

Bellomo, K., Angeloni, M., Corti, S., & von Hardenberg, J. (2021). Future climate change shaped by inter-model differences in Atlantic meridional overturning circulation response. *Nature Communications*, *12*, 3659. https://doi.org/10.1038/s41467-021-24015-w

Bond, G., Broecker, W., Johnsen, S., McManus, J., Labeyrie, L., Jouzel, J., & Bonani, G. (1993). Correlations between climate records from North Atlantic sediments and Greenland ice. *Nature*, *365*, 143–147. https://doi.org/10.1038/365143a0

Böning, C. W., Behrens, E., Biastoch, A., Getzlaff, K., & Bamber, J. L. (2016). Emerging impact of Greenland meltwater on deepwater formation in the North Atlantic Ocean. *Nature Geoscience*, *9*, 523–527. https://doi.org/10.1038/ngeo2740

Broecker, W. S. (1998). Paleocean circulation during the last deglaciation: A bipolar seesaw? *Paleoceanography and Paleoclimatology*, *13*(2), 119–121. https://doi.org/10.1029/97PA03707

Broecker, W. S., Bond, G., Klas, M., Bonani, G., & Wolfli, W. (1990). A salt oscillation in the glacial Atlantic? 1. The concept. *Paleoceanography and Paleoclimatology*, *5*(4), 469–477. https://doi.org/10.1029/PA005i004p00469

Crowley, T. (1992). North Atlantic deepwater cools the southern hemisphere. *Paleoceanography and Paleoclimatology*, *7*(4), 489–497. https://doi.org/10.1029/92PA01058

Danabasoglu, G., Yeager, S. G., Bailey, D., Behrens, E., Bentsen, M., Bi, D., et al. (2014). North Atlantic simulations in coordinated ocean-ice reference experiments phase II (CORE-II). Part I: Mean states. *Ocean Modelling*, *73*, 76–107. https://doi.org/10.1016/j.ocemod.2013.10.005

Danabasoglu, G., Yeager, S. G., Kim, W. M., Behrens, E., Bentsen, M., Bi, D., et al. (2016). North Atlantic simulations in coordinated ocean-ice reference experiments phase II (CORE-II). Part II: Inter-annual to decadal variability. *Ocean Modelling*, *97*, 65–90. https://doi.org/10.1016/j.ocemod.2015.11.007

Dansgaard, W., Johnsen, S., Clausen, H., Dahl-Jensen, D., Gundestrup, N. S., Hammer, C. U., et al. (1993). Evidence for general instability of past climate from a 250-kyr ice core record. *Nature*, *364*, 218–220. https://doi.org/10.1038/364218a0

Devilliers, M., Swingedouw, D., Mignot, J., Deshayes, J., Garric, G., & Ayache, M. (2021). A realistic Greenland ice sheet and surrounding glaciers and ice caps melting in a coupled climate model. *Climate Dynamics*, *57*, 2467–2489. https://doi.org/10.1007/s00382-021-05816-7

Dima, M., Lohmann, G., & Knorr, G. (2018). North Atlantic versus global control on dansgaard-oeschger events. *Geophysical Research Letters*, *45*(23), 12991–12998. https://doi.org/10.1029/2018GL080035

Dokken, T. M., Nisancioglu, K. H., Li, C., Battisti, D. S., & Kissel, C. (2013). Dansgaard-Oeschger cycles: Interactions between ocean and sea ice intrinsic to the Nordic seas. *Paleoceanography and Paleoclimatology*, *28*(3), 491–502. https://doi.org/10.1002/palo.20042

Drijfhout, S., van Oldenborgh, G. J., & Cimatoribus, A. (2012). Is a decline of AMOC causing the warming hole above the north Atlantic in observed and modeled warming patterns? *Journal of Climate*, *25*(24), 8373–8379. https://doi.org/10.1175/JCLI-D-12-00490.1

Golledge, N. R., Keller, E. D., Gomez, N., Naughten, K. A., Bernales, J., Trusel, L. D., & Edwards, T. L. (2019). Global environmental consequences of twenty-first-century ice-sheet melt. *Nature*, *566*, 65–72. https://doi.org/10.1038/s41586-019-0889-9

Gregory, J. M., Griffies, S. M., Hughes, C. W., Lowe, J. A., Church, J. A., Fukimori, I., et al. (2019). Concepts and terminology for sea level: Mean, variability and change, both local and global. *Surveys in Geophysics*, *40*, 1251–1289. https://doi.org/10.1007/s10712-019-09525-z

Haine, T. W. N., Curry, B., Gerdes, R., Hansen, E., Karcher, M., Lee, C., et al. (2015). Arctic freshwater export: Status, mechanisms, and prospects. *Global and Planetary Change*, *125*, 13–35. https://doi.org/10.1016/j.gloplacha.2014.11.013

Hanna, E., Cappelen, J., Fettweis, X., Mernild, S. H., Mote, T. L., Mottram, R., et al. (2021). Greenland surface air temperature changes from 1981 to 2019 and implications for ice-sheet melt and mass-balance change. *International Journal of Climatology*, *41*, E1336–E1352. https://doi.org/10.1002/joc.6771

Hawkins, E., Smith, R. S., Allison, L. C., Gregory, J. M., Woollings, T. J., Pohlmann, H., & de Cuevas, B. (2011). Bistability of the Atlantic overturning circulation in a global climate model and links to ocean fresh water transport. *Geophysical Research Letters*, *38*, L10605. https://doi.org/10.1029/2011GL047208

Hu, A., Meehl, G. A., Han, W., & Yin, J. (2011). Effect of the potential melting of the Greenland ice sheet on the meridional overturning circulation and global climate in the future. *Deep-Sea Research Part II*, *58*(17–18), 1914–1926. https://doi.org/10.1016/j.dsr2.2010.10.069

Jungclaus, J. H., Fischer, N., Haak, H., Lohmann, K., Marotzke, J., Matei, D. D., et al. (2013). Characteristics of the ocean simulations in MPIOM, the ocean component of the MPI-Earth system model. *Journal of Advances in Modeling Earth Systems*, *5*, 422–446. https://doi.org/10.1002/jame.20023

Kageyama, M., Merkel, U., Otto-Bliesner, B., Prange, M., Abe-Ouchi, A., Lohmann, G., et al. (2013). Climatic impacts of fresh water hosing under last glacial maximum conditions: A multi-model study. *Climate of the Past*, *9*(2), 935–953. https://doi.org/10.5194/cp-9-935-2013

Lenton, T. M., Held, H., Kriegler, E., Hall, J. W., Lucht, W., Rahmstorf, S., & Schellnhuber, H. J. (2008). Tipping elements in the Earth's climate system. *Proceedings of the National Academy of Sciences*, *105*(6), 1786–1793. https://doi.org/10.1073/pnas.0705414105

Lenton, T. M., Rockström, J., Gaffney, O., Rahmstorf, S., Richardson, K., Steffen, W., & Schellnhuber, H. J. (2019). Climate tipping points—Too risky to bet against. *Nature*, *575*, 592–595. https://doi.org/10.1038/d41586-019-03595-0

Lohmann, G., Butzin, M., Eissner, N., Shi, X., & Stepanek, C. (2020). Abrupt climate and weather changes across timescales. *Paleoceanography and Paleoclimatology*, *35*(9), e2019PA003782. https://doi.org/10.1029/2019PA003782

Matthes, K., Biastoch, A., Wahl, S., Harlaß, J., Martin, T., Brücher, T., et al. (2020). The flexible ocean and climate infrastructure version 1 (FOCI1): Mean state and variability. *Geoscientific Model Development*, *13*, 2533–2568. https://doi.org/10.5194/gmd-13-2533-2020

Mauritsen, T., Bader, J., Becker, T., Behrens, J., Bittner, M., Brokopf, R., et al. (2019). Developments in the MPI-M Earth system model version 1.2 (MPI-ESM1.2) and its response to increasing CO_2. *Journal of Advances in Modeling Earth Systems*, *11*, 998–1038. https://doi.org/10.1029/2018MS001400

Mouginot, J., Rignot, E., Bjork, A. A., van den Broeke, M., Millan, R., Morlighem, M., et al. (2019). Forty-six years of Greenland Ice Sheet mass balance from 1972 to 2018. *Proceedings of the National Academy of Sciences*, *116*, 9239–9244. https://doi.org/10.1073/pnas.1904242116

NGRIP North Greenland Ice Core Project members. (2004). High-resolution record of Northern Hemisphere climate extending into the last interglacial period. *Nature*, *431*, 147–151. https://doi.org/10.1038/nature02805

Pedro, J. B., Jochum, M., Buizert, C. F., He, F., Barker, S., & Rasmussen, S. O. (2018). Beyond the bipolar seesaw: Toward a process understanding of interhemispheric coupling. *Quaternary Science Reviews*, *192*, 27–46. https://doi.org/10.1016/j.quascirev.2018.05.005

Rahmstorf, S. (2002). Ocean circulation and climate during the past 120,000 years. *Nature*, *419*, 207–214. https://doi.org/10.1038/nature01090

Reick, C. H., Raddatz, T., Brovkin, V., & Gayler, V. (2013). The representation of natural and anthropogenic land cover change in MPI- ESM. *Journal of Advances in Modeling Earth Systems*, *5*(3), 459–482. https://doi.org/10.1002/jame.20022

Rhein, M., Steinfeldt, R., Huhn, O., Sültenfuß, J., & Breckenfelder, T. (2018). Greenland submarine melt water observed in the Labrador and Irminger Sea. *Geophysical Research Letters*, *45*(10), 10570–10578. https://doi.org/10.1029/2018GL079110

Seidov, D., & Maslin, M. (2001). Atlantic ocean heat piracy and the bipolar climate see- saw during Heinrich and Dansgaard-Oeschger events. *Journal of Quaternary Science*, *16*(4), 321–328. https://doi.org/10.1002/jqs.595

Sein, D. V., Koldunov, N. V., Danilov, S., Sidorenko, D., Wekerle, C., Cabos, W., et al. (2018). The relative influence of atmospheric and oceanic model resolution on the circulation of the North Atlantic Ocean in a coupled climate model. *Journal of Advances in Modeling Earth Systems*, *10*, 2026–2041. https://doi.org/10.1029/2018MS001327

Severinghaus, J. P., & Brook, E. J. (1999). Abrupt climate change at the end of the last glacial period inferred from trapped air in polar ice. *Science*, *286*, 930–934. https://doi.org/10.1126/science.286.5441.930

Sidorenko, D., Rackow, T., Jung, T., Semmler, T., Barbi, D., Danilov, S., et al. (2015). Towards multi-resolution global climate modeling with ECHAM6–FESOM. Part I: Model formulation and mean climate. *Climate Dynamics*, *44*, 757–780. https://doi.org/10.1007/s00382-014-2290-6

Stevens, B., Giorgetta, M., Esch, M., Mauritsen, T., Crueger, T., Rast, S., et al. (2013). Atmospheric component of the MPI-M earth system model: ECHAM6. *Journal of Advances in Modeling Earth Systems*, *5*(2), 146–172. https://doi.org/10.1002/jame.20015

Stocker, T. F., & Johnsen, S. J. (2003). A minimum thermodynamic model for the bipolar seesaw. *Paleoceanography and Paleoclimatology*, *18*, 1087. https://doi.org/10.1029/2003PA000920

Stouffer, R. J., Yin, J., Gregory, J. M., Dixon, K. W., Spelman, M. J., Hurlin, W., et al. (2006). Investigating the causes of the response of the thermohaline circulation to past and future climate changes. *Journal of Climate*, *19*, 1365–1387. https://doi.org/10.1175/JCLI3689.1

Swingedouw, D., Rodehacke, C. B., Behrens, E., Menary, M., Olsen, S. M., Gao, Y., et al. (2013). Decadal fingerprints of freshwater discharge around Greenland in a multi-model ensemble. *Climate Dynamics*, *41*, 695–720. https://doi.org/10.1007/s00382-012-1479-9

Swingedouw, D., Rodehacke, C. B., Olsen, S. M., Menary, M., Gao, Y., Mikolajewicz, U., & Mignot, J. (2015). On the reduced sensitivity of the Atlantic overturning to Greenland ice sheet melting in projections: A multi-model assessment. *Climate Dynamics*, *44*, 3261–3279. https://doi.org/10.1007/s00382-014-2270-x

The IMBIE Team. (2020). Mass balance of the Greenland ice sheet from 1992 to 2018. *Nature*, *579*, 233–239. https://doi.org/10.1038/s41586-019-1855-2

WAIS Divide Project Members. (2015). Precise interpolar phasing of abrupt climate change during the last ice age. *Nature*, *520*, 661–665. https://doi.org/10.1038/nature14401

Weijer, W., Cheng, W., Garuba, O. A., Hu, A., & Nadiga, B. T. (2020). CMIP6 models predict significant 21st century decline of the Atlantic meridional overturning circulation. *Geophysical Research Letters*, *47*, e2019GL086075. https://doi.org/10.1029/2019GL086075

References From the Supporting Information

Berk, J. v.d., Drijfhout, S. S., & Hazeleger, W. (2021). Circulation adjustment in the Arctic and Atlantic in response to Greenland and Antarctic mass loss. *Climate Dynamics*, *57*, 1689–1707. https://doi.org/10.1007/s00382-021-05755-3

Griffies, S. M., & Greatbatch, R. J. (2012). Physical processes that impact the evolution of global mean sea level in ocean climate models. *Ocean Modelling*, *51*, 37–72. https://doi.org/10.1016/j.ocemod.2012.04.003

Griffies, S. M., Yin, J., Durack, P. J., Goddard, P., Bates, S. C., Behrens, E., et al. (2014). An assessment of global and regional sea level for years 1993–2007 in a suite of interannual CORE-II simulations. *Ocean Modelling*, *78*, 35–89. https://doi.org/10.1016/j.ocemod.2014.03.004

Jackson, L. C., & Wood, R. A. (2018). Timescales of AMOC decline in response to fresh water forcing. *Climate Dynamics*, *51*, 1333–1350. https://doi.org/10.1007/s00382-017-3957-6

Obase, T., & Abe-Ouchi, A. (2019). Abrupt Bølling-Allerød warming simulated under gradual forcing of the last deglaciation. *Geophysical Research Letters*, *46*(11), 11397–11405. https://doi.org/10.1029/2019GL084675

Rahmstorf, S., Crucifix, M., Ganopolski, A., Goosse, H., Kamenkovich, I., Knutti, R., et al. (2005). Thermohaline circulation hysteresis: A model intercomparison. *Geophysical Research Letters*, *32*(23), L23605. https://doi.org/10.1029/2005GL023655

Ziemen, F. A., Kapsch, M.-L., Klockmann, M., & Mikolajewicz, U. (2019). Heinrich events show two-stage climate response in transient glacial simulations. *Climate of the Past*, *15*, 153–168. https://doi.org/10.5194/cp-15-153-2019